

Advancing Stellar Streams as a Dark Matter Probe — I: Evolution of the CDM subhalo population

Paul Menker,^{1,2*} and Andrew Benson²

¹University of Southern California, 3551 Trousdale Pkwy, Los Angeles, CA 90089, USA

²Observatories, Carnegie Institution for Science, 813 Santa Barbara Street, Pasadena, CA 91101, USA=

Accepted XXX. Received YYY; in original form ZZZ

ABSTRACT

Stellar streams, long thin streams of stars, have been used as sensitive probes of dark matter substructure for over two decades. Gravitational interactions between dark matter substructures and streams lead to the formation of low density “gaps” in streams, with any given stream typically containing no more than a few such gaps. Prior models for the statistics of such gaps have relied on several simplifying assumptions for the properties of the subhalo population in the cold dark matter scenario. With the expected forthcoming increase in the number of streams, and gaps, observed, in this work we develop a more detailed model for the statistics of subhalos interacting with streams, and test some of the assumptions made in prior works. Instead of using simple fits to N-body estimates of subhalo population statistics at $z = 0$ as in previous work, we make use of realizations of time-dependent subhalo populations generated from a fully physical model, incorporating structure formation, and subhalo orbital evolution, including tidal heating and stripping physics, which has been carefully calibrated to match results of cosmological N-body simulations. We find that this model predicts up to 60% more gaps on average in Pal-5-like streams than prior works.

Key words: cosmology: theory, dark matter

1 INTRODUCTION

Stellar streams—long, dynamically cold strings of stars—are created from dwarf galaxies and globular clusters. More specifically, as these progenitor systems orbit in the halos of massive host galaxies, streams are slowly generated through tidal stripping of stars from the progenitor. They were first observed over five decades ago (Eggen 1971; see also Johnston et al. 2002; Ibata et al. 2002), but recent surveys have drastically increased the population and resolution of known streams (Malhan et al. 2018; Price-Whelan & Bonaca 2018). Eccentricities range from nearly circular to as high as 0.7 (Li et al. 2022; Cubarsi et al. 2021). Due to their kinematically cold nature, resulting from adiabatic cooling, streams have very low velocity dispersions, only a few km/s. Therefore, even small perturbations from external sources of gravitational potential can produce observable changes in the stream structure. Typically, through induced changes in the orbital periods of stream member stars, perturbations will lead to the formation of a gap (Erkal & Belokurov 2015a)—a region of lower density in the stream. The Cold Dark Matter (CDM) model predicts overdense dark matter subhalos down to very small mass scales (Giocoli et al. 2008), which can act as perturbers and induce gap formation in streams. These gaps can be used as forensic tools to reconstruct the subhalo “flybys” that occur (Erkal & Belokurov 2015a; Erkal et al. 2016) through both their size and numbers. By extension, the dark matter subhalo population as a whole can be probed statistically, as shown in Yoon et al. (2011). Although the predicted average number of observable gaps in each stream is small (2 gaps in GD-1 for example; Bonaca et al. 2019), by combining gap statistics

of many streams, dark matter models can be constrained (Yoon et al. 2011). Our work is motivated by the recent substantial expansion in the number of known stellar streams, and the expected continued expansion of this population due to new datasets from GAIA (Bonaca & Price-Whelan 2024), the Via project¹, and Roman (Sanderson et al. 2019). As the numbers of known and well-characterized streams grows, it is crucial that the theoretical models of gap formation have the requisite accuracy to allow careful inferences to be made on the particle nature of dark matter.

Extensive work has been performed to understand gap formation in both qualitative and quantitative ways, particularly in Carlberg (2012, 2013), Erkal & Belokurov (2015a) and Erkal et al. (2016). These works analytically modeled the $z = 0$ subhalo population through fits to data from cosmological N-body simulations. In these works, when a subhalo approaches close enough to a stream to create a significant perturbation, the impulse approximation is used to calculate the change in velocity of the stream material, typically utilizing the assumption of a Plummer profile (Plummer 1911) for the subhalo. From these velocity kicks, orbital phase changes are computed, resulting in predictions for later evolution of the orbits of stream member stars, and, therefore, the numbers and depths of gaps induced. In this work, we aim to refine this model, particularly improving upon the assumptions made for the subhalo population. To do so, we will make use of the modular, semi-analytic, simulation framework “GALACTICUS” (Benson 2012). As a semi-analytical framework, GALACTICUS simplifies over direct N-body simulation by working with (sub)halos (rather than particles) as fundamental objects, and solving a coupled

* E-mail: pmenker@usc.edu

¹ <https://via-project.org/>

set of differential equations describing the relevant physics that controls the evolution of those (sub)halos. This allows for a substantially faster calculation of subhalo populations, while retaining the key physical processes (including tidally-induced evolution in subhalo density profiles), and allowing an accurate match to N-body results. Through use of the GALACTICUS framework we model the subhalo population more precisely, account for tidal evolution in the density profiles of subhalos, and evolve it through the lifetime of the stream, accounting for the growth in the length of the stream over time. As we do not seek analytic solutions to the growth of gaps² we also drop several approximations made in prior work, favouring numerical solutions. Details, and the simplifying assumptions that are retained from prior works are discussed in §2.

Similar calculations are being carried out using direct N-body simulation of subhalo populations (Gialluca et al. 2021). These are potentially more accurate than our semi-analytic approach, but are substantially slower, making it much more challenging to generate large numbers of realizations from which to extract statistical predictions for the frequency and properties of gaps. A key advantage of N-body simulations, however, is that they can explore more than just basic gap properties (e.g. size and depth), examining unique features that have been discovered, such as the spur of GD-1 (Bonaca et al. 2019). In principle, full forensic data (e.g. velocities of stars along the stream, and the full 3D shape of the perturbation) can be extracted from our semi-analytic approach. We leave examination of these more detailed predictions to a future work, focusing here on simple statistics (gap size and depth) that are more readily characterized observationally. Other work, such as Bovy et al. (2016) and Banik & Bovy (2019) have modeled other perturbers using power spectrum data.

At present, there are over 120 known stellar streams, with lengths on the order of $\sim 5\text{--}50$ kpc (Erkal et al. 2016; Bovy et al. 2016). Their intrinsic velocity dispersions range from as low as 0.5 km/s for GD-1 (Gialluca et al. 2021), to as high as 20 km/s for Turranburra (Li et al. 2022). Pal-5, upon which we will focus in this work, has an intrinsic velocity dispersion of 1.2 km/s (Kuzma et al. 2015). The number of known streams is expected to greatly increase in the coming years. This calls for a re-examination of previous work on stellar streams as a dark matter probe, as predictions are entirely statistical. With hundreds of streams and $O(1)$ gap per stream, we can expect statistical uncertainties in the mean number of gaps per stream below the 10% level. The challenges of systematic errors are discussed in §4 and §5.

While dark matter subhalos are expected to be the primary perturbers (Yoon et al. 2011; Carlberg 2012; Erkal & Belokurov 2015a), perturbations to streams may also be created by inhomogeneities in the stream progenitor (Bonaca et al. 2019), variations in the rate of tidal mass loss (Carlberg 2020), the Milky Way bar (Pearson et al. 2017), Giant Molecular Clouds (GMCs; Amorisco et al. 2016), and the Large Magellanic Cloud (LMC; Shipp et al. 2021). We do not consider these sources in this work, focusing only on subhalo-induced gaps. Of course, the contributions of these non-subhalo perturbers will be important to understand before gap statistics can be used to place constraints on the subhalo population.

This paper is laid out as follows. In §2, we review the gap formation

framework, much of the relevant analytic theory, and our implementation of the GALACTICUS simulation suite, highlighting differences from previous work. In §3, predictions of gap sizes and number are presented. In §4, these results are compared to previous work, and the various strengths and shortcomings are discussed. Finally, in §5, these results are summarized, and applications to future work are laid out.

2 METHODS

2.1 Stellar Streams

Conceptually, the gap formation mechanism is as follows: dark matter subhalos represent a perturbation to the smooth gravitational potential of the host halo, and as these objects fly close to the stream they therefore perturb the trajectories of individual stars. These perturbations are strongest closest to the subhalo itself (because of the inverse square nature of gravitational accelerations), such that each piece of the stream receives a different velocity “kick”. These differential velocity kicks lead to the formation of an underdense region around the site of the impact. A clear underdense gap can form from a sufficiently massive (or sufficiently close) perturbation. In this work we consider only subhalos with time of closest approach bound masses between $10^5 M_\odot$ and $10^9 M_\odot$. We will demonstrate that this range is sufficient to capture all significant gap contribution from cuspy subhalos.

We consider three different density profiles to describe the gravitational potential of subhalos: a Plummer model (Plummer 1911; Aarseth et al. 1974), an NFW profile (Navarro et al. 1997), and a tidally stripped and heated NFW profile (Peñarrubia et al. 2008; Erani & Peñarrubia 2020; Benson & Du 2022). The Plummer model has been used in previous work (Erkal & Belokurov 2015a; Erkal et al. 2016) where its simple form allows for analytic calculations of velocity kicks and phase shifts, and is an improvement over a point mass (Yoon et al. 2011; Carlberg 2013). An NFW profile, while not allowing for analytical integration of velocity kicks, is a much more accurate model of halo structure. During halo assembly, accreted halos oftentimes have their outer density profile strongly perturbed by the tidal field of their host halo, resulting in “tidally stripped” subhalos. Additionally, gravitational tidal shocks can heat the inner regions of the subhalo, leading to further changes in the density profile (Gnedin et al. 1999). We will refer to these as “tidally stripped NFW” profiles. The NFW and tidally stripped NFW profiles are “cuspy” profiles and are expected to produce stronger perturbations during close encounters as more of their mass is concentrated into the dense center.

As explained by Erkal & Belokurov (2015a; see their Figure 1), gap formation can be split into three qualitatively distinct phases. First the gravitationally-induced velocity kicks in the stream cause a “compression” phase, where the stream material concentrates toward the point of impact of the subhalo, resulting in a density enhancement in the stream of magnitude $f \equiv \rho/\rho_0 > 1$, with (ρ being the stream density, ρ_0 being its unperturbed value). This phase exists for a timescale on the order of Myrs, and is then replaced by an expansion phase, where $f \leq 1$ in the central region. Finally on timescales of several tens of Gyrs, caustics form, where particles from close to the point of impact, with large velocity kicks overtake those further out, resulting in extremely large density spikes. For an idealized stream, caustic densities would be infinite, but the velocity dispersion and discreteness of stream material (stars) dampens the spikes. In Erkal & Belokurov (2015a), much of the focus was on the “expansion” phase,

² In earlier works, e.g. Erkal & Belokurov (2015a), the use of Plummer sphere profiles for subhalos allowed analytic solutions for velocity kicks to be found. In our approach, using tidally-evolved CDM density profiles no such analytic solutions exist. Therefore, we are forced to proceed numerically, and so there is no advantage in making other, simplifying assumptions needed to retain a fully-analytical approach.

as these constitute the majority of observable gaps in the universe. However, in this work, as we solve for the evolution of the perturbed stream numerically, all phases of gap formation are simulated³.

2.2 Generating Subhalo Populations

Every gravitationally accurate realization of a galaxy must include its dark matter halo, and all the substructure contained within. Because dark matter is not directly observable, and so can not be fully mapped within our galaxy⁴, one must model its presence statistically to make predictions about gaps. To make accurate and statistically-representative predictions we generate random realizations of subhalo populations using a physics based approach. Specifically, we make use of the GALACTICUS semi-analytic model (Benson 2012) to predict the assembly and orbital evolution (and eventual destruction) of populations of subhalos without the computational cost of full N-body modelling. For a full description of how GALACTICUS models subhalo physics we refer the reader to Pullen et al. (2014), Yang et al. (2020) and Benson & Du (2022).

Briefly, GALACTICUS starts from a Milky Way-mass ($10^{12}M_{\odot}$), halo at $z = 0$, and constructs the assembly history of that halo by building a merger tree using the algorithm of Parkinson et al. (2008), resolving progenitor halos down to a mass of 10^5M_{\odot} . Using our concentration model Johnson et al. (2021) we find these Milky Way halos to have a median concentration of $c = 8.33$ at $z = 0$. For computational efficiency we do not follow every branch of the tree, but instead subsample branches. This allows us to avoid having to track the evolution of huge numbers of low mass halos, while having only a small number of higher mass halos. Specifically, at each branching of the merger tree, we randomly decide whether or not to follow the lower mass branch with probability

$$p(M) = \begin{cases} (M/10^9M_{\odot}) & \text{if } M < 10^9M_{\odot}, \\ 1 & \text{if } M \geq 10^9M_{\odot}, \end{cases} \quad (1)$$

where M is the mass of the lower mass branch. Of course, this subsampling affects the statistics of subhalo-stream interactions which we wish to calculate in this work. To correct for this we evaluate a weight, w_i , for each halo/subhalo which accounts for this subsampling. When a branching occurs in the merger tree, and the branch is retained, we assign the halo in that branch a weight $w_i = w_j/p(M_i)$ where w_j is the subsampling weight of the parent halo, M_i is the mass of the new branch, and $w_1 = 1$ (the weight of the root halo in the tree). We have verified that, when applying these subsampling weights, this approach results in a distribution of subhalo masses that precisely matches the original, non-sampled algorithm.

Each halo in the resulting merger tree is assumed to be described by an NFW density profile⁵ (Navarro et al. 1997), with a virial density contrast given by the spherical collapse model (as appropriate to the dark energy cosmological model used in this work; Eke et al. 1996; Percival 2005), and a concentration determined using the model of Johnson et al. (2021) which computes the NFW scale radius from

each halo’s assembly history⁶. Halo spins are determined from the assembly history of each halo using the model of Benson et al. (2020).

The halos in each merger tree are then evolved forward in time. When two halos in the tree merge, the lower mass halo becomes a subhalo in the higher mass halo. As the tree continues to evolve more and more halos merge, resulting in a population of subhalos (and sub-subhalos, etc.). GALACTICUS follows the orbital evolution of each subhalo in the time evolving potential of its host halo. Initial orbital parameters are assigned from the cosmological distribution measured by Jiang et al. (2015; with best fit parameter values as determined by Benson et al. (2020) and including the correlation with the host halo spin as found by those authors) at the time of merging. The orbital motion is then integrated forward in time including the effects of dynamical friction, tidal stripping, and tidal heating (Pullen et al. 2014). The latter modifies the original density profile of a subhalo according to a simple heating model (Benson & Du 2022).

If a halo containing subhalos merges into a yet larger halo, thereby becoming a subhalo itself, the original subhalos are now sub-subhalos. These sub-subhalos remain bound to their original host halo (and continue to orbit within it) until and unless they stray outside the instantaneous tidal radius of that host. When this happens, the sub-subhalo (which we will refer to as halo “A”) is assumed to be tidally stripped from their subhalo host (halo “B”), and becomes a subhalo in the host halo (halo “C”) of halo B, with an initial position and velocity equal to the vector sum of the orbital position/velocity of A in B, plus the orbital position/velocity of the B in C. At any given time, GALACTICUS thereby provides full details (current bound masses, orbital positions and velocities, density profiles) of all subhalos orbiting within the Milky Way halo. This model has been calibrated to accurately match subhalo mass functions and radial distributions measured from cosmological N-body simulations (Yang et al. 2020, see also Nadler et al. 2023b), and to match the evolution of tidally-heated halos in idealized simulations (Benson & Du 2022). As such, it provides an accurate and detailed description of cosmological subhalo populations.

For this work, we perform dark matter only-simulations—all baryonic physics is switched off in GALACTICUS such that no galaxies are formed. This allows for comparison with earlier works which were based on fits to dark matter-only N-body simulations. Of course, GALACTICUS is able to incorporate a detailed treatment of galaxy formation physics, which may have important implications for subhalo populations and the statistics of gaps in stellar streams (see §4 for further discussion of this point).

To model the time evolution of the subhalo population, GALACTICUS models subhalos as tidally stripped NFW density profiles. For the other density profiles that we consider (Plummer and NFW) the profiles are constructed from the subhalo masses tracked by GALACTICUS including all tidal effects. Thus, changing the density profile does not change the distributions of subhalo masses or orbital parameters. This allows us to isolate the effects of changing the density profile alone.

For this work, we focus on the Pal-5 stream (Starkman et al. 2020).

³ Of course, the timescales for the compression and caustic phases are such that the majority of gaps are observed in the expansion phase.

⁴ Of course, larger dark matter substructures—such as the subhalo hosting the LMC—can be measured with reasonable precision, such that their effects can be accounted for directly (Shipp et al. 2021). We will comment further on this in §4.

⁵ Using an Einasto (1965) density profile would provide a slightly more accurate description of the distribution of mass in halos (Navarro et al. 2004; Gao et al. 2008; Hayashi & White 2008). However, the current GALACTICUS model is calibrated assuming NFW halos, so we retain that assumption here.

⁶ This concentration calculation can, in principle, be affected by our choice to subsample branches of the merger tree, as it uses the properties of merging halos to compute the evolution of concentration. The algorithm is constructed such that contributions from branches that are ignored due to subsampling are still approximately accounted for in the mean evolution of the concentration. We find that the actual effect of subsampling on this aspect of our model is weak. For example, we find that the mean concentration of the Milky Way halo is shifted by only 0.08 dex when we include subsampling, while there is almost no change in the halo-to-halo variance in the concentration.

We generate 4,000 merger tree realizations of our Milky Way galaxy’s halo, taking snapshots of the subhalo population at 3000 timesteps, with timesteps evenly spaced between the stream’s formation and the present. Pal-5 is 3.4 Gyr old (Küpper et al. 2015), 9 kpc long (Grillmair & Dionatos 2006), and at an average distance of 13 kpc (Odenkirchen et al. 2003) from the Galactic center, with length growing approximately linearly in time⁷. Because the timestep Δt , between simulations is of order 1 Myr, which is much less than the dynamical time in the halo, our subhalo population is well-resolved in time. Each timestep contains exhaustive information about the subhalos present, in particular their existence, mass, orbital position and velocity, subsampling weight (as described above), concentration, and virial radius, which are used for our NFW model. Additionally, for each subhalo, a tabulated density profile is output which describes the tidally stripped NFW profile. From this data, several calculations are performed. First, the population is cleaned of any halos that are not subhalos of the main branch of the merger tree⁸. Then, because we assume that the subhalo population is not correlated with the orientation of the stream, we can freely rotate the system⁹. This effectively increases the sample size of subhalos that interact strongly with the stream, and is performed for 400 isotropically random rotations. Additionally, taking further advantage of this isotropy of the subhalo system in the simulated mass range, the stream is extended from an arc to a full circle for the purposes of finding close encounters with subhalos (the resulting gap statistics will be weighted accordingly to the actual length of the stream at each snapshot, by multiplying the contribution of each gap by a factor of $l(t)/2\pi r_0$, where $l(t)$ is the length of the stream as a function of time, and r_0 is the orbital radius of the stream). Note that the Plummer, NFW, and tidally stripped NFW profiles all use the same populations generated here, and differ only in the density profiles of their subhalos.

2.3 Calculating Gap Sizes

For each subhalo (in each merger tree realization, random rotation, and at each timestep) we now have sufficient information to compute the interaction between that subhalo and the stream, and so find the properties of the gap induced in the stream. Our approach mostly follows that of Erkal & Belokurov (2015a), differing only when we resort to numerical techniques, which is frequent for the NFW and tidally-stripped NFW profiles.

Each “flyby”, when a subhalo passes near to the stream, can be thought of as scattering event. In particular, we employ an impulse approximation where the stream is considered to be fixed in position during the scattering event, and further assume that the momentum imparted to stars in the stream is much less than their initial momenta. The resulting velocity kick is then found by simply integrating the gravitational acceleration caused by the perturber over time:

$$\Delta \mathbf{v} = \int_{-\infty}^{\infty} \mathbf{a} dt. \quad (2)$$

As our subhalo density profiles are assumed to be spherically sym-

⁷ See, for example, Figure 2 of Bovy et al. (2016). We ignore the oscillations in stream length due to the eccentricity of the stream orbit as, in this work, we approximate the stream with a circular orbit.

⁸ At times $z > 0$ the outputs from our simulations also include halos and subhalos that have not yet merged into the Milky Way progenitor halo. These are excluded as they, by definition, can not have a close encounter with the stream in the Milky Way progenitor halo at this time.

⁹ This will no longer be true when baryons are included in the simulation.

metric this can be written as:

$$\Delta \mathbf{v} = \int_{-\infty}^{\infty} \frac{GM(r)}{r^2} \hat{\mathbf{r}} dt, \quad (3)$$

where $M(r)$ is the subhalo mass enclosed within a radius r , taken to be the magnitude of the vector \mathbf{r} connecting a point in the stream to the center of the subhalo, and a hat over a vector indicates the corresponding unit vector. Defining $\hat{\mathbf{y}}$ to be the direction of the stream, with $y = 0$ corresponding to the point of closest approach, and $\hat{\mathbf{x}}$ to be pointing radially outward from the Galactic center, we can define $r(t)$ for a particular segment of stream a distance y away from the point of closest approach. Defining \mathbf{w} to be the relative *initial* velocity between stream and perturber (when the calculation is instantiated), and b as the impact parameter (i.e. the distance of closest approach between the subhalo and the stream), it is straightforward to see that:

$$r(t) = \sqrt{(y + w_{\parallel}t)^2 + w_{\perp}^2 t^2 + b^2}, \quad (4)$$

where $w_{\parallel} \equiv \mathbf{w} \cdot \hat{\mathbf{y}} = v_{y,\text{subhalo}} - v_{\text{stream}}$, and $\mathbf{w}_{\perp} \equiv (v_{x,\text{subhalo}}, 0, v_{z,\text{subhalo}})$. We note that $r(0) = \sqrt{y^2 + b^2} = b$ when $y = 0$, the impact parameter/distance of closest approach. Furthermore, $r(-t_{\text{impact}}) = \sqrt{x_0^2 + (y_0 - r_{\text{stream}}) + z_0^2}$, the relative distance between the stream and perturber when the simulation is instantiated, where t_{impact} is the time from the start of the simulation until the time of closest approach. This model is agnostic to dark matter particle physics (assuming no dark matter–baryon interactions)—one can accommodate any dark matter candidate by changing the subhalo population and $M(r)$ in equation (3). In this work we will focus only on CDM subhalo populations, and remind the reader that for Plummer, NFW, and tidally stripped NFW profiles, we use same CDM subhalo population. We now describe in detail each of these three models.

The Plummer sphere is a useful toy model due to the availability of analytic solutions to many of the relevant integrals. It is defined by the potential

$$\Phi_{\text{Plummer}}(r) = -\frac{GM_b}{\sqrt{r^2 + r_p^2}}, \quad (5)$$

where M_b is the total bound mass of the object, and the *Plummer radius* r_p acts as a smoothing parameter. At small distances ($r \lesssim r_p$), r_p avoids numerical singularities, while at large distances ($r \gg r_p$), a Plummer potential approaches the potential of a point mass. During a flyby, the stream only interacts with $M(< r)$, which has the form

$$M(r) = M_b \frac{r^3}{(r^2 + r_p^2)^{3/2}}. \quad (6)$$

For comparison with Erkal et al. (2016) we adopt their choice of

$$r_p = 1.62 \text{ kpc} \left(\frac{M_b}{10^8 M_{\odot}} \right)^{1/2} \quad (7)$$

when using Plummer profiles. Thus, for a Plummer sphere, one can deduce

$$\begin{aligned} \Delta v_x &= \int_{-\infty}^{\infty} \frac{GM_b (b_x + w_x t)}{\left((y + w_{\parallel}t)^2 + w_{\perp}^2 t^2 + b^2 + r_p^2 \right)^{3/2}} dt \\ &= \frac{2GM_b \left(b w^2 \cos \alpha + y w_{\perp} w_{\parallel} \sin \alpha \right)}{w \left((b^2 + r_p^2) w^2 + w_{\perp}^2 y^2 \right)} \end{aligned} \quad (8)$$

where $b_x = b \cos \alpha$, $b_z = b \sin \alpha$, and one can equate $v_{x,\text{subhalo}} =$

$w_x, v_{z,\text{subhalo}} = w_z$ because $\mathbf{v}_{\text{stream}} = (0, v_{\text{stream}}, 0)$. Similar equations can be deduced for Δv_y and Δv_z .

The well known NFW profile, by contrast, has been empirically fit to N-body simulations, providing a simple, yet accurate model of the density in a CDM halo. It is defined by (Navarro et al. 1997)

$$\rho = \frac{\rho_0}{(r/r_s)(1+r/r_s)^2}, \quad (9)$$

where ρ_0 is an overall normalization of the density profile. The scale radius, r_s , governs the transition from a shallow $\sim 1/r$ density profile at $r \lesssim r_s$, and a steeper $\sim 1/r^3$ scaling at $r \gg r_s$. The NFW profile is “cuspy,” meaning that it has a diverging central density. This leads to stronger scattering at small b , and thus we expect NFW profiles to produce more gaps (of a given size and depth) than a “cored” Plummer model. Both ρ_0 and r_s are computed in GALACTICUS for each subhalo as described above. Following the formalism of equation (3), one finds

$$\Delta v_x = 4\pi\rho_0 r_s^3 G \int_{-\infty}^{\infty} \frac{\log(1+r/r_s) - \frac{r}{r+r_s}}{r^3} (b_x + w_x t) dt, \quad (10)$$

and similarly for Δv_y and Δv_z . Note that for large r , $M(r)$ can exceed the current bound mass, M_b , of the subhalo as predicted by GALACTICUS’ tidal stripping model. We therefore limit $M(r)$ to never exceed M_b . Generally, this expression for Δv_x is not analytically integrable for an NFW profile. We therefore evaluate the integral numerically for 200 points in y along the stream. These points were concentrated around $y = 0$ to ensure that small gap sizes could be computed accurately, but extended to an angle of 200° in either direction¹⁰.

During the formation of the Galactic halo, much of the mass of infalling subhalos is stripped away (as evidenced by the low mass-fraction in subhalos, e.g. Gao et al. 2011), and tidal heating modifies the distribution of the mass that remains bound (Peñarrubia et al. 2008; Errani & Peñarrubia 2020; Benson & Du 2022). The resulting “tidally stripped NFW profiles” cannot be represented by any simple analytic form. Therefore, GALACTICUS outputs the resulting mass profile, $M(r)$, for each subhalo at a set of 10 radii chosen to sample the radii of interest (i.e. spanning from well within the scale radius out to the virial radius of each subhalo).

Regardless of the model, equation (3) allows one to compute the perturbed velocity of any point along the stellar stream. In principle these velocity kicks themselves are observable through spectroscopic analysis. Recent work suggests that such spectroscopic data, coupled with photometric observations, could be crucial to distinguish dark matter induced gaps from other sources by constraining the time and velocity of the gap-inducing encounter (Erkal & Belokurov 2015b). However, as photometric data of gap sizes will be available for large samples before large spectroscopic surveys we choose to focus purely on photometric properties (gap sizes and depths) in this work.

The velocity kicks cause a change in the orbital angle, $\theta(t)$, of a particular section of stream. Following the angular velocity conservation arguments of Erkal & Belokurov (2015a), one finds

$$\theta(t) \left(1 + \frac{\Delta v_y}{v_y} \frac{4 - \gamma^2}{\gamma^2} \right) - 4 \frac{\Delta v_y}{v_y} \frac{\sin(\gamma\theta(t))}{\gamma^3} + 2 \frac{\Delta v_x}{v_x} \frac{1 - \cos(\gamma\theta(t))}{\gamma^2} = \frac{v_y}{r_0} t, \quad (11)$$

where r_0 is the radius of the stream, $\phi(r)$ is the gravitational potential

of the stream’s host halo, and $\gamma^2 = 3 + \frac{r_{\text{stream}}^2}{v_y^2} \partial_r^2 \phi(r_{\text{stream}}) = 2$ for flat rotation curves as assumed by Erkal & Belokurov (2015a). We also adopt $\gamma^2 = 2$ in this work even though our host halo has an NFW profile, for which γ^2 varies with radius. This is necessary as, currently, our simulations are dark matter only, and therefore miss the contribution of the Milky Way Galaxy to $\phi(r)$. In future work we intend to incorporate baryonic physics into our model, allowing us to compute γ^2 directly (see §4 for further discussion of this point).

Equation (11) is true to leading order in $\Delta v_y/v_y$, which is of order 1% or less for typical encounters. Previous work switched variables to $\Delta\theta(t) = [\theta(t) - v_y t]/r_0$ and Taylor expanded to generate an analytical form. However, given that gaps can exceed 100° , and that $\Delta\mathbf{v}$ cannot be solved analytically for the NFW models anyway, all results in this work employ a numerical solution of equation (11). If we define the initial position of any piece of the stream to be $\theta_0 = y/r_0$, these particles will move both due to the 0th order motion of the stream¹¹, and because of the variable velocity kick each portion of the stream receives. Thus,

$$\theta(\theta_0, t) = \theta_0 + \Delta\theta(\theta_0, t). \quad (12)$$

This is both a tautological restatement of the fact that there is a perturbed and unperturbed contribution to the angle of the stream, and one of the most powerful tools of this formulation. Through equations (11) and (12), one can track the evolution of every point of the stream. Because of mass conservation and the treatment of streams as one dimensional lines, we can define

$$f \equiv \frac{\rho_{\text{stream}}}{\rho_{0,\text{stream}}} = \left| \frac{\partial\theta(t)}{\partial\theta_0} \right|^{-1}, \quad (13)$$

or

$$f = 1 + \frac{\partial\Delta\theta(t)}{\partial\theta_0}. \quad (14)$$

The other key parameter is the width of a gap at a given depth, $\Delta\theta$. This is determined by calculating $f(\theta)$, and finding the width of a region where $f < f_{\text{cut}}$, where f_{cut} represents an upper limit of detectability for a gap that will depend on the specific observational survey.

2.4 Overview of Workflow

Having developed the necessary formalism we now briefly review the overall workflow, and describe how we exclude from our calculations subhalos that do not produce gaps of sufficient size or depth to be of interest. Excluding such subhalos from our calculations results in a substantial increase in computational efficiency.

We begin by using GALACTICUS to generate subhalo populations for 4,000 separate realizations of a Milky Way halo, snapshotting the population at 3,000 timesteps between the present day and the time at which the stream formed. To each realization we apply 400 independent, isotropically-distributed random rotations. We then apply various cuts to exclude subhalos that will not contribute to the formation of significant gaps.

First, as previously explained, any halo that is not a subhalo of the Milky Way progenitor halo is removed. Next, we eliminate any subhalo that will not reach its point of closest approach to the stream

¹⁰ This of course exceeds a full circle, but allows us to interpolate accurately up to any desired angle.

¹¹ This is not a perfect approximation at large angles, but most gaps are localized near the point of closest approach.

in the current timestep, or has already passed that point (and is therefore moving away from the stream).

At this point, Δv_x and Δv_y integrals are computed on a logarithmically-spaced set of 200 y values for each subhalo, timestep and rotation. For subhalos with impact parameter, b , greater than the subhalo's outer radius (calculated by interpolating in the radii of the subhalo's tidally stripped bound mass), subhalos are treated as a point mass, allowing an analytic solution¹², drastically reducing computation time. As any stream will have an intrinsic velocity dispersion, any event with a maximum Δv_y significantly smaller than this dispersion will result in a perturbation that is indistinguishable from noise, and so should be excluded, following the logic of [Erkal et al. \(2016\)](#). The total velocity dispersion of Pal-5 is 1.2 km/s ([Kuzma et al. 2015](#)), which is typical of comparable streams ([Gialluca et al. 2021](#)). Therefore, we make a conservative cut by excluding any subhalo for which the maximum $\Delta v_y < 0.1$ km/s.

For subhalos remaining after these cuts, $\Delta\theta$ and $f(\theta)$ are computed. To compute a gap size, one has to define an f_{cut} (the threshold below which a gap is identified). We consider several different values of f_{cut} . In future work, f_{cut} can be chosen to match the specifics of any observational survey/stream. For each value of f_{cut} we find the maximum extent, $\Delta\theta$, for which $f(\theta) < f_{\text{cut}}$ and identify this as the gap size.

Finally, gap statistics (e.g. the mean number of gaps per stream, the distribution of gap sizes, etc.) are found by averaging over all realizations and rotations, and summing over all timesteps. As mentioned in §2.2, low mass subhalos are subsampled to increase simulation speed. Therefore, when summing over subhalo contributions to any statistics we include the weight, w_i (see eqn. 1), to account for this subsampling. Additionally, as we treat the stream as a full circle at all times (which allows us to exploit the spherical symmetry of our model to increase the number of close encounters), we weight each gap's contribution by a factor proportional to the actual length of the stream at the time of the encounter as described in §2.2 as the probability of any encounter will be proportional to the length of the stream.

3 RESULTS

We now apply our model to compute statistical properties of the distribution of gaps in streams. For all results presented here our model is applied to a specific stream, Pal-5, which we take to be 3.4 Gyr old ([Küpper et al. 2015](#)), 9 kpc long at the present time ([Grillmair & Dionatos 2006](#)), and at an average distance of 13 kpc ([Odenkirchen et al. 2003](#)) from the Galactic center. We begin, in §3.1, by comparing properties of the subhalo population to the previous analytical work [Erkal et al. \(2016\)](#). In §3.2 and §3.3, we then examine the predicted distribution of gap sizes and the number of gaps per stream respectively.

3.1 Subhalo Population Properties

Figures 1–3 show distributions of key properties of the subhalo population, comparing results from this work with those adopted by [Erkal et al. \(2016\)](#). The comparison is made at $z = 0$ —in this work the subhalo population evolves over time, while in [Erkal et al. \(2016\)](#) these distributions did not evolve, but were fixed to measurements from

¹² Specifically, for a point mass, the kick velocity is given by equation 8 in the limit $r_p \rightarrow 0$ as the Plummer profile has finite total mass.

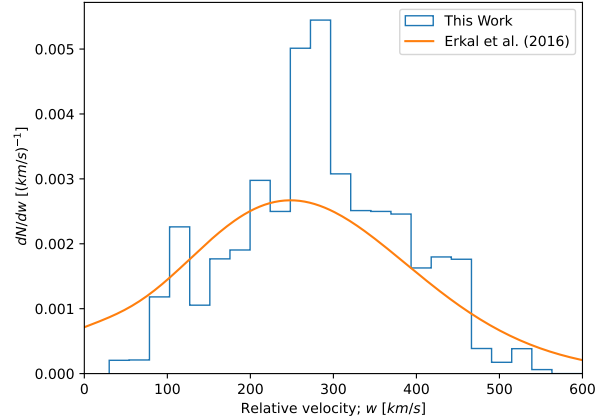


Figure 1. The distribution of relative velocities between subhalos and the stream at redshift $z \approx 0$. All infalling subhalos within 2.5 kpc of the stream were included. The orange line shows the distribution used by ([Erkal et al. 2016](#)), their equations 5–7, which predict relative velocities of *infalling* subhalos. The blue line shows results from this work, also for infalling subhalos, averaged over all realizations of the Milky Way halo.

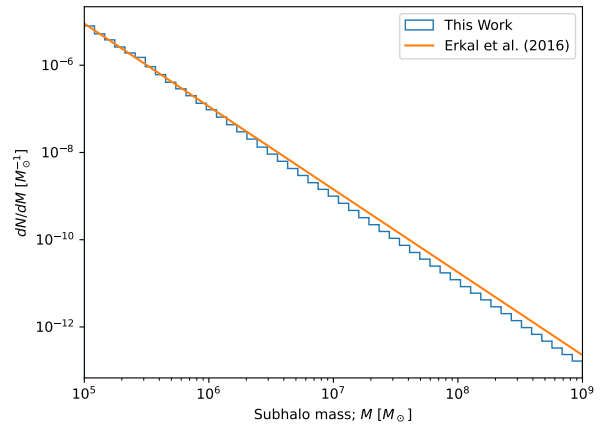


Figure 2. The distribution of present-day subhalo bound masses (i.e. the subhalo mass function) at redshift $z = 0$. All subhalos within the Milky Way halo are included. The orange line shows the distribution used by [Erkal et al. \(2016\)](#), while the blue line shows results from this work, averaged over all realizations of the Milky Way halo.

N-body simulations at $z = 0$. Figure 1 plots the distribution of relative velocities of the subhalos with respect to the stream, including only subhalos that are infalling, and within 2.5 kpc of the stream (as was used by [Erkal et al. \(2016\)](#) in estimating this distribution). The selection of subhalos that are undergoing their closest approach with the stream results in a bias toward higher relative velocities. [Erkal et al. \(2016\)](#) account for this bias in constructing their distribution function. In this work, to match this bias, only subhalos making their closest approach to the stream in the timestep being considered are counted. There is overall good agreement between the distribution predicted by GALACTICUS and that adopted by [Erkal et al. \(2016\)](#), although the distribution from GALACTICUS is slightly less broad.

Next, Figure 2 shows the distribution of subhalo masses, both from this work and [Erkal et al. \(2016\)](#). All subhalos within the Milky Way

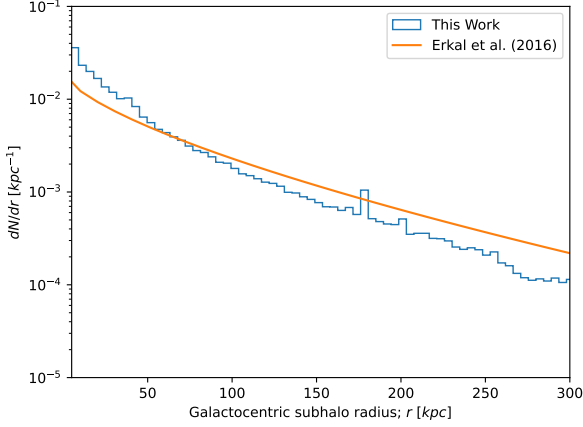


Figure 3. The distribution of the galactocentric radii of subhalos at redshift $z = 0$. All subhalos with bound masses $10^5 M_\odot < M_b < 10^9 M_\odot$ were included. The orange line shows the distribution used by Erkal et al. (2016), while the blue line shows results from this work, averaged over all realizations of the Milky Way halo.

halo are included (i.e. there is no selection on radial position, or of infalling subhalos). The small spike at $M = 3 \times 10^5 M_\odot$ is due to a random fluctuation, enhanced in amplitude by our subsampling approach, and is therefore not physical. The results from this work agree very closely with those from Erkal et al. (2016), as is to be expected as GALACTICUS is known to accurately match subhalo mass functions from N-body simulations (Yang et al. 2020) to which Erkal et al. (2016) calibrated their model.

Finally, Figure 3 shows the radial distribution of subhalos with masses in the range $10^5 M_\odot < M_b < 10^9 M_\odot$ (and without any selection of infalling subhalos). “Spikes” in the results from GALACTICUS are again due to random fluctuations enhanced by our subsampling approach. The overall shape predicted by GALACTICUS is somewhat different from that adopted by Erkal et al. (2016), with Galacticus predicting a subhalo population that is more centrally-concentrated than that used by Erkal et al. (2016).

This difference in the shape of the radial distribution of subhalos as predicted by Galacticus and by N-body simulations has also been noted by Nadler et al. (2023b), who compared Galacticus predictions matched to their “Symphony” suite of zoom-in N-body simulations. Galacticus was not calibrated to match the radial distribution of subhalos (instead being calibrated to match subhalo mass functions and the subhalo V_{\max} – M relation; Yang et al. 2020)—further calibration in this statistic may improve the agreement with N-body simulations. However, as noted by Nadler et al. (2023b), Galacticus’ predictions agree with the Symphony N-body results within the 2σ statistical uncertainties of those simulations. Furthermore, as also discussed by Nadler et al. (2023b), subhalo radial distributions measured from N-body simulations may be affected by numerical issues, such as subhalo “withering” (van den Bosch et al. 2017) and artificial disruption (Errani & Navarro 2021). Improved subhalo finder algorithms (Mansfield et al. 2023), and higher resolution simulations may help to resolve these issues in the near future, allowing for a more accurate assessment of the subhalo radial distribution.

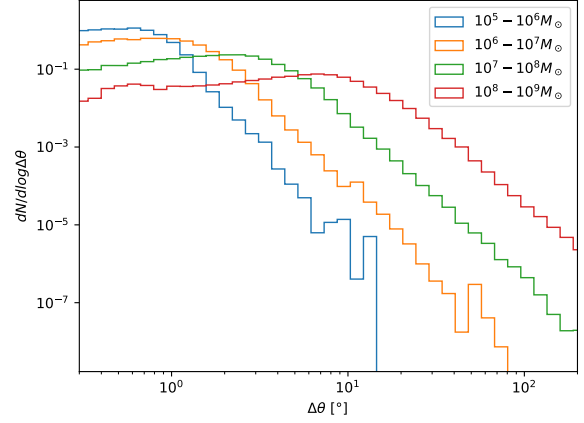


Figure 4. The distribution of gap sizes, $\Delta\theta$, derived assuming tidally stripped NFW profiles is shown for four intervals of subhalo mass from $10^5 M_\odot$ to $10^9 M_\odot$ as indicated in the figure. For this figure, gaps are defined using a threshold of $f_{\text{cut}} = 0.5$.

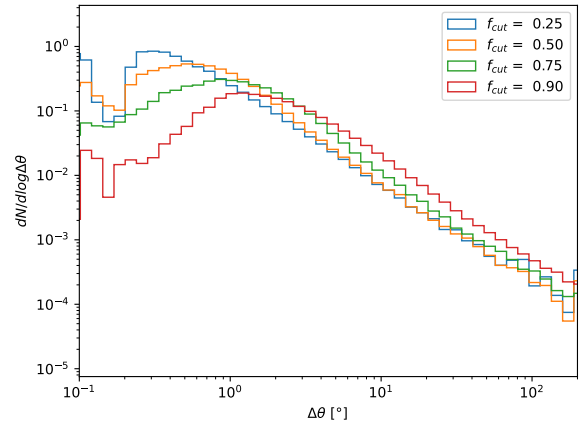


Figure 5. The distribution of gap sizes, $\Delta\theta$, derived assuming tidally stripped NFW profiles is shown for four different thresholds f_{cut} as indicated in the figure. Subhalos with masses in the range $10^5 M_\odot < M_b < 10^9 M_\odot$ are included.

3.2 Gap Sizes

Figures 4–6 present predicted distributions of gap sizes in the Pal-5 stream, generated using the model described in §2. Figure 4 presents distributions split by subhalo mass, assuming tidally stripped NFW profiles, and are defined using a density threshold of $f_{\text{cut}} = 0.5$. As subhalo masses increase the distribution of gap sizes is shifted toward larger values, as expected (more massive subhalos causes stronger perturbations, leading to larger gaps).

Figure 5 presents similar distributions, but here all subhalo masses are included in each curve. Each curve shows results for a different choice of density threshold, f_{cut} , as indicated in the figure. For smaller values of f_{cut} (corresponding to the selection of deeper gaps) the distribution of gap sizes is shifted toward smaller values.

Finally, Figure 6 presents normalized gap size distributions for different choices of dark matter subhalo density profile, as indicated in the figure. In all cases a density threshold of $f_{\text{cut}} = 0.5$ is used, and

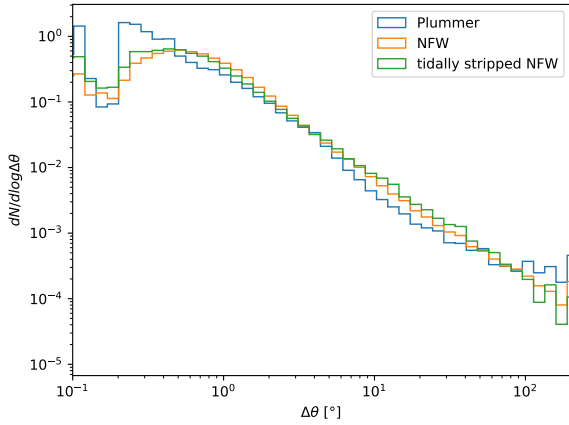


Figure 6. The distribution of gap sizes, $\Delta\theta$, computed under different models for the dark matter subhalo density profile, as indicated in the figure. Subhalos with masses in the range $10^5 M_\odot < M_b < 10^9 M_\odot$ are included, and gaps are defined using a threshold of $f_{\text{cut}} = 0.5$.

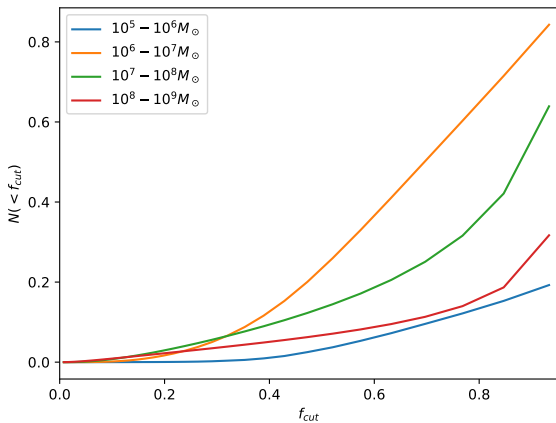


Figure 7. The mean number of gaps of size greater than 1° per Pal-5 stream as a function of the threshold, f_{cut} , originating from encounters with subhalos in different mass intervals (as indicated in the figure).

contributions from subhalos over the entire mass range ($10^5 M_\odot < M_b < 10^9 M_\odot$) are included. While the distributions are quite similar for all density profile models ($< 1\%$ of subhalo-stream interactions have impact parameters small enough to probe the inner structure of the subhalo), there is a clear excess of gaps in the $3\text{--}10^\circ$ size interval when using an NFW or tidally stripped NFW profile relative to when a Plummer profile is used. While it is only an $\mathcal{O}(2)$ difference, this is significant when using streams as a dark matter probe.

3.3 Number of Predicted Gaps

Figures 7–8 show the predicted mean number of gaps of size greater than 1° per Pal-5 stream as a function of gap depth threshold, f_{cut} . As stated previously, the number of gaps in Pal-5 depends on the minimum depth observable by current photometric and spectroscopic data. When shallower gaps are included, the total number of gaps naturally increases. We choose $f_{\text{cut}} = 0.5$ as a representative value, but results can be computed for any choice of threshold. In both

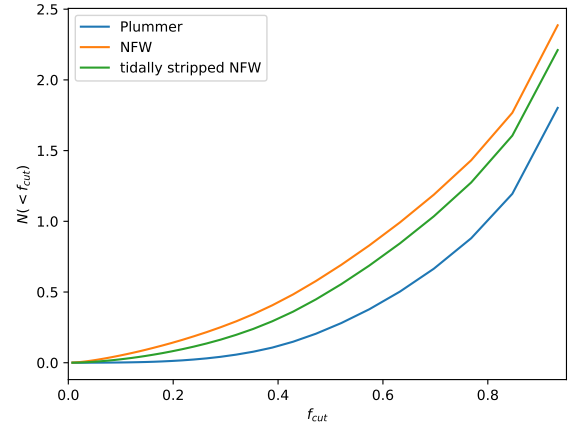


Figure 8. The mean number of gaps of size greater than 1° per Pal-5 stream as a function of the threshold, f_{cut} , is shown for three different models of the subhalo density profile. Subhalos across the entire mass range considered ($10^5 M_\odot < M_b < 10^9 M_\odot$) are included.

f_{cut}	0.10	0.20	0.30	0.50	0.75	0.90
Plummer	0.002	0.013	0.047	0.247	0.821	1.509
NFW	0.052	0.143	0.264	0.642	1.365	2.091
Truncated	0.024	0.083	0.174	0.508	1.210	1.923
Erkal et al. (2016)	—	—	—	0.300	0.700	—

Table 1. The mean number of gaps of size greater than 1° per Pal-5 stream is shown for different thresholds, f_{cut} (columns), and for different choices for the subhalo density profile (rows), and including contributions from subhalos across the entire mass range of $10^5 M_\odot < M_b < 10^9 M_\odot$. In the final row we show results quoted by [Erkal et al. \(2016\)](#) where available.

figures we assume tidally stripped NFW density profiles for subhalos. In Figure 7 the mean number of gaps is split into contributions from four intervals of subhalo mass, as indicated in the figure. The number of gaps contributed per decade of subhalo mass peaks in the $10^6 M_\odot$ to $10^7 M_\odot$ interval. For higher masses the number of gaps contributed is reduced simply because these higher mass subhalos are far less abundant, while for lower masses the number of gaps is reduced because, while there are many such subhalos, interactions with sufficiently small impact parameter to generate wide and deep gaps become exceedingly rare.

Figure 8 also shows the predicted mean number of gaps $> 1^\circ$ per Pal-5 stream as a function of gap depth threshold, f_{cut} , but now including contributions from subhalos of all masses. Individual lines correspond to different choices for the subhalo density profile as indicated in the figure. The cuspy NFW and tidally stripped NFW profiles produce more gaps (or given depth and size) than the cored Plummer profile, due to their more concentrated mass distributions. Tidal truncation and heating of the NFW profiles causes a modest, $\sim 8\%$ reduction in the total number of gaps produced.

These same results are tabulated in Table 1 for a few values of f_{cut} . We also quote the results given by [Erkal et al. \(2016\)](#) where available. These should be compared with our results for a Plummer profile—there is close agreement between our results and those of [Erkal et al. \(2016\)](#) in these cases. The differences (which are at the level of 20%) arise from the differences in subhalo population statistics (see §3.1),

the evolution of the subhalo population over time (included in our model, but not in that of Erkal et al. 2016) and, to a much lesser degree, are use of numerical solutions to eqn. (11) instead of a series expansion solution.

4 DISCUSSION

The results presented in §3 show that the improvements developed in this work result in significant changes to gap predictions. While, the $z = 0$ subhalo population remains largely unchanged from the previous work of Erkal et al. (2016) aside from radial distribution, there are significant differences at the level of 0.05–0.10 gaps per stream for the Plummer model. From this, we can infer that the treatment of time evolution in the subhalo population, cosmologically-motivated distribution of subhalo orbits, and the resulting radial distribution of subhalos collectively have a non-negligible impact on the number of gaps produced.

Figure 4 confirms that larger mass subhalos contribute to larger gaps, as predicted by the linear mass dependence in eqn. 3. Gaps can, in principle, be arbitrarily small, which is reflected here, where Erkal et al. (2016) predicted no gaps smaller than $\sim 7^\circ$ ¹³. While gaps from high mass subhalos can be $> 100^\circ$ in length, gaps created by lower mass subhalos are, typically, much smaller. For a low mass subhalo to create a large gap, it must have both a small impact parameter, *and* a very small relative velocity with the stream. By passing by the stream at very low speed, there is more time for the subhalo to interact with the stream material. It is unclear if, in these maximally perturbing events from low mass subhalos, the impulse approximation is still valid. However, given how infrequent such interactions are (there are 10^4 times more 1° gaps than 10° gaps for the lowest mass decade), this is unlikely to significantly affect predictions for the total number of gaps with potentially observable sizes and depths. It is, however, reason to relax the impulse approximation in future work.

In Figure 5, which shows how the distribution of gap sizes depends on the threshold f_{cut} , the curves for $f_{\text{cut}} = 0.25$ and $f_{\text{cut}} = 0.50$ begin to overlap above 3° , suggesting that large gaps are also relatively deep. Our results here are qualitatively similar to those of (Erkal et al. 2016, their Figure 13)¹⁴, with differences at small gap size arising from our use of tidally stripped NFW profiles, and at large gap size from our use of numerical solutions to eqn. (11) rather than a series expansion solution.

Figure 6 shows that Plummer, NFW, and tidally stripped NFW density profile models all have relatively similar gap distributions, although the cuspy profiles produce a clear excess in the 3– 10° range. This independence of the results on the subhalo density profile results from the fact that only encounters with sufficiently small impact parameter will probe the internal structure of the subhalo. However, enough small impact parameter encounters occur that there is some significant difference between the results of using different density profiles.

Figure 8 (and Table 1) show that cuspy subhalo density profiles

result in an increase of around 60% in the predicted mean number of gaps per stream, due to the dense center of a cuspy profile which drives larger velocity kicks (and so larger, deeper gaps) during encounters with small impact parameter. Accounting for tidal effects on the NFW profile slightly weakens this effect, but there remains a clear increase in the number of gaps relative to a cored Plummer profile. Of course, the tidally stripped NFW profile is the most realistic case considered here, as it accounts for the known physical processes of tidal stripping and heating.

Rerunning simulations with the position and velocity distributions matching that of Erkal et al. (2016), but all other parameters (including the subhalo mass function) determined as in §2, we find significantly lower gap content, with (0.14, 0.50) gaps predicted at $f_{\text{cut}} = (0.50, 0.75)$ for a Truncated profile, while for a Plummer Profile, we find (0.15, 0.54) gaps at the same cutoff depths. This is in line with Figure 3, which shows that Erkal et al. (2016) predicts fewer subhalos at radii less than 60 kpc. This suggests that the other differences of this paper relative to Erkal et al. (2016) *increase* gap content by a factor of roughly two, as seen in Table 1.

We have treated the stream orbit as circular. To estimate the magnitude of any possible systematic shifts in results associated with this assumption we repeat our calculations at the apocenter and pericenter of Pal-5’s orbit (19.5 kpc and 5.7 kpc respectively; Odenkirchen et al. 2003), using the Truncated subhalo profiles. We find that this gives (0.36, 0.66) gaps at pericenter, and (0.43, 1.24) gaps at apocenter for $f_{\text{cut}} = (0.50, 0.75)$. This suggests very little change in the gap content of any stream ranging from 13–19 kpc, but a more notable change at smaller radii. However, the reader should note that *deep* gap content (gaps with $f_{\text{cut}} \leq 0.30$) remains relatively unchanged, as changes in both subhalo number density (less numerous) and velocity (slower) appear somewhat cancel out. Further more, any systematic bias may be expected to shift more toward the results at apocenter (where the stream stars spend most of their time).

Figure 7 shows a key result relevant to the application of stream gaps to studies of the nature of dark matter: a sizable contribution to the number of gaps from the lowest mass subhalos. Many viable alternatives to CDM (e.g. thermal warm dark matter, models with self-interactions, and axion models) result in suppression of the (sub)halo mass function at low masses. Therefore, probes that are sensitive to lower mass subhalos are expected to set more stringent constraints on such models. Subhalos in the mass range of 10^5 to $10^6 M_\odot$ contribute around 10% of the total number of gaps of size greater than 1° at $f_{\text{cut}} = 0.5$.

Statistically, the results presented in this work are *precise* to approximately 1.0% given the number of realizations (and rotations) of subhalo populations used. However, the *accuracy* of the model, which may be limited by systematic biases is much more difficult to assess. Plausibly the largest systematic bias may arise from the lack of inclusion of baryons in our model¹⁵. In particular, the contribution of the Milky Way galaxy to the gravitational potential and tidal field could have significant consequences for the population of subhalos in the inner regions of the halo (Garrison-Kimmel et al. 2017; Despali & Vegetti 2017; Chua et al. 2017; Nadler et al. 2018, 2021). Beyond this effect, other systematic biases likely remain in our model due to its assumption of spherical symmetry in the subhalo population, the use of a circular orbit for the stream, and the fact that we average over all possible formation histories of a Milky Way-mass halo, rather than only over those consistent with constraints on the formation history

¹³ This was due to Erkal et al. (2016)’s use of an approximate, series solution for $\Delta\theta$ and a Plummer profile for subhalos. The exact minimum gap size in their model is subhalo mass-dependent, but is around 7° for subhalos of mass $10^7 M_\odot$.

¹⁴ Note that Erkal et al. (2016) show histograms normalized to the number of gaps with $f_{\text{cut}} = 0.9$, while we show the distribution function for each f_{cut} —i.e. each curve in our Figure 5 is normalized to unit integral, while those in Figure 13 of Erkal et al. (2016) are not. Therefore, the normalizations of the curves can not be compared, but their shapes can be.

¹⁵ Note that we fix the parameter γ in eqn. (11) to $\gamma^2 = 2$ appropriate to the flat rotation curve of the actual Milky Way (i.e. including baryons).

of the actual Milky Way (e.g. the presence of the Large Magellanic Cloud is uncommon in Milky Way-mass halos, but is known to affect the dynamics of stellar streams; [Shipp et al. 2021](#)).

5 CONCLUSION

Stellar streams are a potentially powerful new probe of dark matter substructure, and therefore of dark matter particle physics. In this work, we build upon prior analytical work ([Erkal & Belokurov 2015a](#); [Erkal et al. 2016](#)) by utilizing a full physics modeling approach to the population of CDM subhalos that cause gap formation. This allows us to account for the evolution of the subhalo population, and to use realistic density profiles (tidally stripped and heated NFW profiles) in our calculations.

We have focused on computing gap statistics for the Pal-5 stream, but our approach is easily generalized to other streams. We find that these improvements result in a prediction for the mean number of gaps (of size greater than 1° at a density threshold of $f_{\text{cut}} = 0.5$) that is around 60% larger than prior estimates.

Our approach is based on Monte Carlo realisations of subhalo populations, but is able to reach precisions of better than 1%. Given typical numbers of ~ 1 gap per stream, with the ~ 100 known streams ([Mateu 2023](#)) the mean number of gaps per stream can potentially be constrained to a precision of ~ 0.1 . Future surveys of ~ 1000 streams ([Aganze et al. 2023](#)) would reduce this to ~ 0.03 . Our model precision is therefore sufficient to meet the requirements of such surveys.

Systematic uncertainties in our predictions remain to be fully explored. A likely source of significant systematic bias is the lack of baryonic physics in our models. Our framework, built using the GALACTICUS galaxy formation model, has the capability to include baryonic physics. This is an area that we intend to explore in future work, allowing us to assess the impact of, for example, the tidal field of the Milky Way on predicted gap statistics.

Other approximations that may lead to systematic biases in our results include our treatment of the stream as being on a circular orbit. For non-circular orbits, some of the symmetries that we exploit to increase computational efficiency will vanish, but beyond this there is no reason why our approach can not be extended to such cases¹⁶. The non-circularity of stream paths leads to oscillations in gap size ([Bovy et al. 2016](#); [Erkal & Belokurov 2015a](#)) and a dependence of where gaps form along the stream.

Our assumption of an isotropic distribution of subhalos is also imperfect. Halos are known to be significantly triaxial, which will affect the orbits and spatial distribution of subhalos. The GALACTICUS toolkit already contains modules to compute halo triaxiality ([Menker & Benson 2022](#)), and we intend to exploit this in future work to further improve our model. Additional anisotropy applies in the specific case of the Milky Way (or, potentially, other galaxies for which we have some knowledge of halo substructure), due to the presence of the Large Magellanic Cloud ([Shipp et al. 2021](#)). In future work, we intend to account for this anisotropy (and other known events in the formation history of the Milky Way) by constructing realizations of merger trees constrained to match these features of the Milky Way ([Nadler et al. 2023a](#)).

As our primary goal in this work is to understand the potential of stellar streams to place constraints on the particle nature of dark

matter, we intend to extend our analysis to other common dark matter candidates (e.g. thermal warm dark matter, self-interacting models), which are implemented in the GALACTICUS framework. We further intend to compute expectations for gap statistics in all known streams. Lastly, while we have not explored it in this work, our model also makes clear predictions for the perturbation in velocity along the stream due to subhalo encounters. This aspect of the model can be exploited to understand the additional constraining power that may arise from spectroscopic studies of streams.

ACKNOWLEDGEMENTS

We thank Ana Bonaca, Denis Erkal, and the entire Streams 2023 conference for inspiration, references, and clarifying discussions. We also thank Ethan Nadler and Sachi Weerasooriya for helpful comments that improved the clarity of this work.

DATA AVAILABILITY

The data underlying this article will be shared on reasonable request to the corresponding author.

REFERENCES

- Aarseth S. J., Hénon M., Wielen R., 1974, *A&A*, **37**, 183
- Aganze C., Pearson S., Starkenburg T., Contardo G., Johnston K. V., Tavanagar K., Price-Whelan A. M., Burgasser A. J., 2023, *arXiv e-prints*, p. [arXiv:2305.12045](#)
- Amorisco N. C., Gómez F. A., Vegetti S., White S. D. M., 2016, *MNRAS*, **463**, L17
- Banik N., Bovy J., 2019, *Mon. Not. Roy. Astron. Soc.*, **484**, 2009
- Benson A. J., 2012, *New Astron.*, **17**, 175
- Benson A. J., Du X., 2022, *MNRAS*, **517**, 1398
- Benson A., Behrens C., Lu Y., 2020, *MNRAS*, **496**, 3371
- Bonaca A., Price-Whelan A. M., 2024, *arXiv e-prints*, p. [arXiv:2405.19410](#)
- Bonaca A., Hogg D. W., Price-Whelan A. M., Conroy C., 2019, *ApJ*, **880**, 38
- Bovy J., Erkal D., Sanders J. L., 2016, *Monthly Notices of the Royal Astronomical Society*, **466**, 628
- Carlberg R. G., 2012, *The Astrophysical Journal*, **748**, 20
- Carlberg R. G., 2013, *The Astrophysical Journal*, **775**, 90
- Carlberg R. G., 2020, *The Astrophysical Journal*, **889**, 107
- Chua K. T. E., Pillepich A., Rodríguez-Gómez V., Vogelsberger M., Bird S., Hernquist L., 2017, *Monthly Notices of the Royal Astronomical Society*, **472**, 4343
- Cubarsi R., Stojanović M., Ninković S., 2021, *A&A*, **649**, A48
- Despali G., Vegetti S., 2017, *MNRAS*, **469**, 1997
- Eggen O. J., 1971, *Publications of the Astronomical Society of the Pacific*, **83**, 271
- Einasto J., 1965, *Trudy Astrofizicheskogo Instituta Alma-Ata*, **5**, 87
- Eke V. R., Cole S., Frenk C. S., 1996, *MNRAS*, **282**, 263
- Erkal D., Belokurov V., 2015a, *Monthly Notices of the Royal Astronomical Society*, **450**, 1136
- Erkal D., Belokurov V., 2015b, *Monthly Notices of the Royal Astronomical Society*, **454**, 3542
- Erkal D., Belokurov V., Bovy J., Sanders J. L., 2016, *Monthly Notices of the Royal Astronomical Society*, **463**, 102
- Errani R., Navarro J. F., 2021, *Monthly Notices of the Royal Astronomical Society*, **505**, 18
- Errani R., Peñarrubia J., 2020, *MNRAS*, **491**, 4591
- Gao L., Navarro J. F., Cole S., Frenk C. S., White S. D. M., Springel V., Jenkins A., Neto A. F., 2008, *MNRAS*, **387**, 536
- Gao L., Frenk C. S., Boylan-Kolchin M., Jenkins A., Springel V., White S. D. M., 2011, *MNRAS*, **410**, 2309

¹⁶ As we already rely on numerical solutions to the equations for gap growth, incorporating the extra terms to account for non-circular motion is not a fundamental difficulty.

- Garrison-Kimmel S., et al., 2017, *MNRAS*, **471**, 1709
- Gialluca M. T., Naidu R. P., Bonaca A., 2021, *The Astrophysical Journal Letters*, 911, L32
- Giocoli C., Tormen G., van den Bosch F. C., 2008, *MNRAS*, **386**, 2135
- Gnedin O. Y., Lee H. M., Ostriker J. P., 1999, *The Astrophysical Journal*, 522, 935
- Grillmair C. J., Dionatos O., 2006, *ApJ*, **641**, L37
- Hayashi E., White S. D. M., 2008, *MNRAS*, **388**, 2
- Ibata R. A., Lewis G. F., Irwin M. J., Quinn T., 2002, *Monthly Notices of the Royal Astronomical Society*, 332, 915
- Jiang L., Cole S., Sawala T., Frenk C. S., 2015, *MNRAS*, **448**, 1674
- Johnson T., Benson A. J., Grin D., 2021, *ApJ*, **908**, 33
- Johnston K. V., Spergel D. N., Haydn C., 2002, *ApJ*, **570**, 656
- Kuzma P. B., Da Costa G. S., Keller S. C., Maunder E., 2015, *MNRAS*, **446**, 3297
- Küpper A. H. W., Balbinot E., Bonaca A., Johnston K. V., Hogg D. W., Kroupa P., Santiago B. X., 2015, *The Astrophysical Journal*, 803, 80
- Li T. S., et al., 2022, *The Astrophysical Journal*, 928, 30
- Malhan K., Ibata R. A., Martin N. F., 2018, *MNRAS*, **481**, 3442
- Mansfield P., Darragh-Ford E., Wang Y., Nadler E. O., Wechsler R. H., 2023, *arXiv e-prints*, p. arXiv:2308.10926
- Mateu C., 2023, *MNRAS*, **520**, 5225
- Menker P., Benson A., 2022, *MNRAS*, **516**, 4383
- Nadler E. O., Mao Y.-Y., Wechsler R. H., Garrison-Kimmel S., Wetzel A., 2018, *The Astrophysical Journal*, 859, 129
- Nadler E. O., Banerjee A., Adhikari S., Mao Y.-Y., Wechsler R. H., 2021, *The Astrophysical Journal Letters*, 920, L11
- Nadler E. O., Benson A., Driskell T., Du X., Gluscevic V., 2023a, *MNRAS*, **521**, 3201
- Nadler E. O., et al., 2023b, *ApJ*, **945**, 159
- Navarro J. F., Frenk C. S., White S. D. M., 1997, *ApJ*, **490**, 493
- Navarro J. F., et al., 2004, *MNRAS*, **349**, 1039
- Odenkirchen M., et al., 2003, *The Astronomical Journal*, 126, 2385
- Parkinson H., Cole S., Helly J., 2008, *MNRAS*, **383**, 557
- Peñarrubia J., Navarro J. F., McConnachie A. W., 2008, *ApJ*, **673**, 226
- Pearson S., Price-Whelan A. M., Johnston K. V., 2017, *Nature Astronomy*, **1**, 633
- Percival W. J., 2005, *A&A*, **443**, 819
- Plummer H. C., 1911, *MNRAS*, **71**, 460
- Price-Whelan A. M., Bonaca A., 2018, *ApJ*, **863**, L20
- Pullen A. R., Benson A. J., Moustakas L. A., 2014, *ApJ*, **792**, 24
- Sanderson R., et al., 2019, *BAAS*, **51**, 347
- Shipp N., et al., 2021, *The Astrophysical Journal*, 923, 149
- Starkman N., Bovy J., Webb J. J., 2020, *MNRAS*, **493**, 4978
- Yang S., Du X., Benson A. J., Pullen A. R., Peter A. H. G., 2020, *MNRAS*, **498**, 3902
- Yoon J. H., Johnston K. V., Hogg D. W., 2011, *The Astrophysical Journal*, 731, 58
- van den Bosch F. C., Ogiya G., Hahn O., Burkert A., 2017, *Monthly Notices of the Royal Astronomical Society*, 474, 3043

This paper has been typeset from a $\text{\TeX}/\text{\LaTeX}$ file prepared by the author.